

Strain-sensitive superconductivity in kagome metals KV_3Sb_5 and CsV_3Sb_5 probed by point-contact spectroscopy

Lichang Yin,^{1,2,*} Dongting Zhang,^{1,2,*} Chufan Chen,^{1,2} Ge Ye,^{1,2} Fanghang Yu,³ Brenden R. Ortiz,⁴ Shuaishuai Luo,^{1,2} Weiye Duan,^{1,2} Hang Su,^{1,2} Jianjun Ying,³ Stephen D. Wilson,⁴ Xianhui Chen,^{3,5,6} Huiqiu Yuan,^{1,2,6,7} Yu Song,^{1,2,†} and Xin Lu^{1,2,6,‡}

¹Center for Correlated Matter and Department of Physics, Zhejiang University, Hangzhou, 310058, China

²Zhejiang Province Key Laboratory of Quantum Technology and Device,
Department of Physics, Zhejiang University, Hangzhou 310058, China

³Hefei National Laboratory for Physical Sciences at Microscale and Department of Physics,
and CAS Key Laboratory of Strongly-coupled Quantum Matter Physics,
University of Science and Technology of China, Hefei, Anhui 230026, China

⁴Materials Department and California Nanosystems Institute,
University of California Santa Barbara, Santa Barbara, CA, 93106, United States

⁵CAS Center for Excellence in Quantum Information and Quantum Physics, Hefei, Anhui 230026, China

⁶Collaborative Innovation Center of Advanced Microstructures, Nanjing 210093, China

⁷State Key Laboratory of Silicon Materials, Zhejiang University, Hangzhou 310058, China
(Dated: June 28, 2021)

The kagome lattice is host to flat bands, topological electronic structures, Van Hove singularities and diverse electronic instabilities, providing an ideal platform for realizing highly tunable electronic states. Here, we report soft- and mechanical- point-contact spectroscopy (SPCS and MPCS) studies of the kagome superconductors KV_3Sb_5 and CsV_3Sb_5 . Compared to the superconducting transition temperature T_c from specific heat measurements (2.8 K for CsV_3Sb_5 and 1.0 K for KV_3Sb_5), significantly enhanced values of T_c are observed via the zero-bias conductance of SPCS (~ 4.2 K for CsV_3Sb_5 and ~ 1.8 K for KV_3Sb_5), which become further enhanced in MPCS measurements (~ 5.0 K for CsV_3Sb_5 and ~ 3.1 K for KV_3Sb_5). While the differential conductance curves from SPCS are described by a two-gap s -wave model, a single s -wave gap reasonably captures the MPCS data, likely due to a diminishing spectral weight of the other gap. The enhanced superconductivity probably arises from local strain caused by the point-contact, which also leads to the evolution from two-gap to single-gap behaviors in different point-contacts. Our results demonstrate highly strain-sensitive superconductivity in kagome metals CsV_3Sb_5 and KV_3Sb_5 , which may be harnessed in the manipulation of possible Majorana zero modes.

PACS numbers:

I. INTRODUCTION

Due to its unique geometry, the kagome lattice natively hosts electronic flat bands, Dirac band crossings, and Van Hove singularities, allowing for the realization of distinct topological electronic states^{1–4} and correlated collective orders^{5–10}. The recent discovery of superconductivity in the kagome metals AV_3Sb_5 ($A = K, Rb, Cs$)^{11–14} triggered immense interest, as superconductivity in these materials coexist with topologically protected surface states¹² and an unusual chiral charge order^{15,16}, offering an ideal platform to investigate the interplay between these exotic phenomena and their evolution upon tuning.

While the nature of superconducting pairing in AV_3Sb_5 is still under debate^{17–21}, signatures of spin-triplet supercurrent were found in $K_{1-x}V_3Sb_5$ Josephson junctions²², and possible Majorana zero modes have been detected in CsV_3Sb_5 ²³. These findings raise the possibility that AV_3Sb_5 may exhibit topological superconductivity with potential applications in fault-tolerant quantum computation^{24,25}. Superconductivity in AV_3Sb_5 is highly susceptible to pressure, displaying two superconducting domes in the temperature-pressure phase diagram^{17,26–30}, and a roughly triple enhancement

of the superconducting transition temperature T_c can be realized under modest pressures of ≈ 1 GPa. The tunability of superconductivity under pressure suggests that it may be modulated by strain, for example to induce superconductor-metal transitions or to stabilize superconductor-metal heterostructures, and raises prospects for the strain-manipulation of possible Majorana zero modes.

In this work, we applied soft and mechanical point-contact spectroscopy (SPCS and MPCS) to investigate the superconducting properties of single crystalline CsV_3Sb_5 and KV_3Sb_5 . From both temperature- and field-dependence of the zero-bias conductance, as well as analyses of the differential conductance curves $G(V)$ with the Blonder-Tinkham-Klapwijk (BTK) model, we observed that values of T_c in SPCS and MPCS are substantially enhanced relative to those from thermodynamic measurements. The enhancement of superconductivity is attributed to local strain in the point-contact region, consistent with the larger enhancement observed in MPCS. While describing the differential conductance from SPCS requires two s -wave gaps, a single gap is sufficient to capture the MPCS results. Nonetheless, the anomalously small ratio

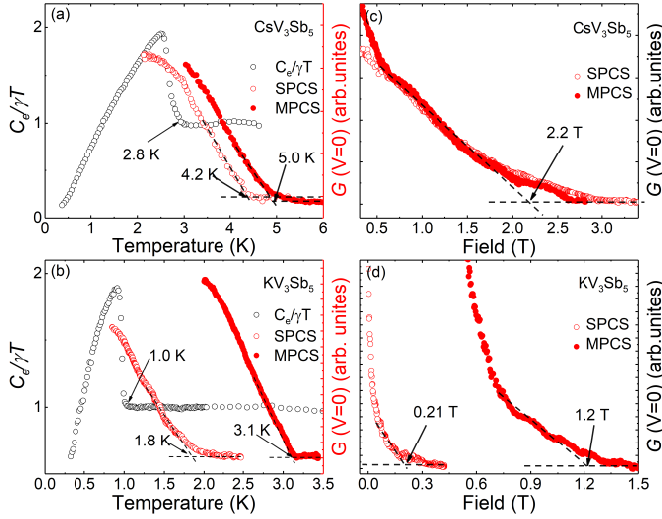


FIG. 1: Temperature dependence of the electronic specific heat $C_e(T)/\gamma T$ and zero-bias conductance $G(V=0)$ measured using SPCS and MPCS for (a) CsV_3Sb_5 and (b) KV_3Sb_5 . $C_e(T)/\gamma T$ data for CsV_3Sb_5 and KV_3Sb_5 are respectively from Ref.¹⁸ and Ref.²⁷. Field-dependence of the zero-bias conductance $G(V=0)$ measured using SPCS and MPCS at $T = 0.3$ K for (c) CsV_3Sb_5 and (d) KV_3Sb_5 , with the field along the c -axis. The arrows mark the onset of superconductivity.

between the superconducting gap and T_c in the MPCS results suggests the presence of an undetected larger gap. Our results demonstrate highly strain-sensitive superconductivity in the kagome metals KV_3Sb_5 and CsV_3Sb_5 , and provide evidence for nodeless multi-gap pairing.

II. EXPERIMENTAL DETAILS

High quality single crystals of CsV_3Sb_5 and KV_3Sb_5 were synthesized using the self-flux method^{12,13}. SPCS measurements were performed by attaching a gold wire (30 μm in diameter) onto cleaved samples through a drop of silver paint, forming hundreds of parallel nanoscale conducting channels between individual silver particles and the sample surface. The contact areas have diameters in the range 50 – 100 μm . MPCS measurements were carried out in an anvil-needle configuration, where electrochemically etched gold tips are employed and piezo-controlled nano-positioners are used to gently control the engagement between the tip and the sample. Differential conductance as a function of the bias voltage $G(V)$ was recorded with the lock-in technique in a quasi-four-probe configuration. An Oxford Instruments cryostat with a ^3He insert (base temperature 0.3 K) was used for SPCS and MPCS measurements, and magnetic fields up to 3.5 T were applied along the c -axis.

III. RESULTS

A. Zero-bias conductance

In Fig. 1(a), the zero-bias conductance $G(V=0)$ from SPCS and MPCS measurements are compared with the electronic specific heat $C_e(T)/\gamma T$ for CsV_3Sb_5 . In contrast to superconductivity that onsets below $T_c \approx 2.8$ K in $C_e(T)/\gamma T$, the temperature dependence of $G(V=0)$ for CsV_3Sb_5 indicates an onset of Andreev reflection below ≈ 4.2 K for SPCS and ≈ 5.0 K for MPCS, suggesting the T_c probed by point-contact spectroscopy is significantly enhanced. Similar behaviors are observed in KV_3Sb_5 , with a $T_c \approx 1.0$ K in $C_e(T)/\gamma T$ increased to ≈ 1.8 K for SPCS and ≈ 3.1 K for MPCS, as shown in Fig. 1(b). It should be emphasized that while signatures of superconductivity from both Andreev reflection [Figs. 1(a) and (b)] and resistivity onset at higher temperatures relative to $C_e(T)/\gamma T$ measurements^{12,13}, they are distinct because (1) the onset temperature from Andreev reflection is even higher than that from resistivity, and (2) it increases systematically from SPCS to MPCS in both CsV_3Sb_5 and KV_3Sb_5 .

Instead, given that enhanced superconductivity is not observed in scanning tunneling microscopy measurements^{23,31}, the increase of T_c from Andreev reflection in Figs. 1(a)-(b) likely results from effects of point-contacts on the sample. Since superconductivity in AV_3Sb_5 is highly responsive to pressure^{17,26–30}, local strain induced by point-contacts may be responsible for the enhanced superconductivity. The observation of a larger tuning effect in MPCS relative to SPCS is consistent with this scenario, since mechanical point-contacts typically lead to a larger strain compared to soft point-contacts. The enhanced superconductivity also manifests through increased upper critical fields H_{c2} at $T = 0.3$ K ($H \parallel c$): it is ≈ 0.21 T for SPCS and ≈ 1.2 T for MPCS measurements on KV_3Sb_5 [Fig. 1(d)]. In CsV_3Sb_5 , we find $H_{c2} \approx 2.2$ T ($H \parallel c$) for both SPCS and MPCS [Fig. 1(c)], significantly higher than $H_{c2} \approx 1.0$ T determined from resistivity measurements³².

B. Differential conductance curves from SPCS

To probe the superconducting state with enhanced T_c , we systematically measured the differential conductance curves $G(V)$ for CsV_3Sb_5 and KV_3Sb_5 at various temperatures and under different magnetic fields, with SPCS results in Figs. 2-4, and MPCS results in Figs. 5-6. A representative set of SPCS $G(V)$ curves at 0.3 K for CsV_3Sb_5 are shown in Figs. 2(a)-(c), while those for KV_3Sb_5 are shown in Figs. 2(d)-(f). All the conductance curves for CsV_3Sb_5 show a double-peak feature around 0.5 mV and a small bulge around 1 mV, characteristic of two-gap superconductivity. A single-gap s -wave BTK model fails to describe the $G(V)$ curves, with substantial

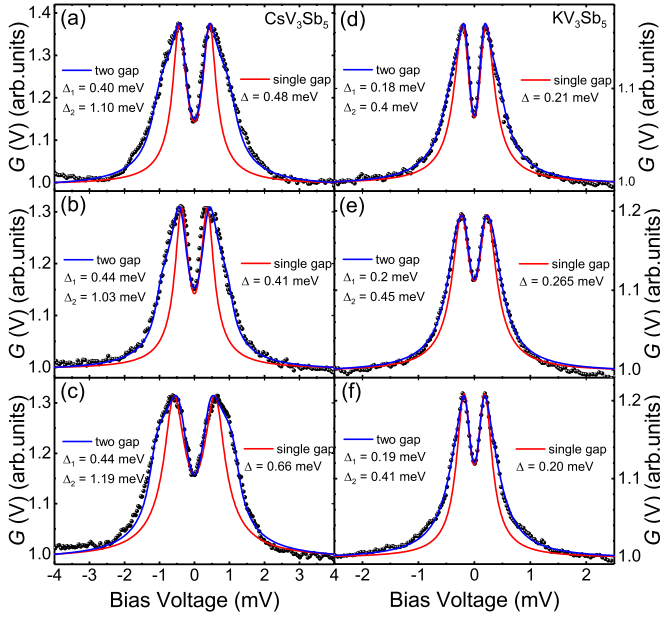


FIG. 2: Representative normalized SPCS differential conductance curves for (a)-(c) CsV_3Sb_5 and (d)-(f) KV_3Sb_5 at $T = 0.3$ K. Solid red lines are fits to a single-gap s -wave model for data with voltages below the peak in $G(V)$. The solid blue lines are fits to a two-gap s -wave model. The slight deviation of the measured differential conductance from the fits at large bias voltages is due to current heating effects³³.

deviations of the fits from experimental data. On the other hand, a two-band BTK model, $G(V) = \omega G_1(V) + (1 - \omega)G_2(V)$ ($0 \leq \omega \leq 1$), with a small ($\Delta_1 \sim 0.4$ meV) and a large gap ($\Delta_2 \sim 1.1$ meV) captures the experimental data, shown as solid blue lines in Figs. 2(a)-(c). ω ranges from 60%-80%, indicating that the small gap exhibits a dominant spectral weight. Similarly, we find that the differential conductance $G(V)$ curves for KV_3Sb_5 from SPCS [solid red line in Figs. 2(d)-(f)] cannot be satisfactorily captured by a single-gap s -wave model. On the other hand, the data can be consistently described by a two-gap s -wave model with $\Delta_1 \sim 0.18$ meV and $\Delta_2 \sim 0.38$ meV, with ω in the range of 20%-70%. Our results suggest that despite enhanced gap values induced by local strain in our SPCS measurements, the superconducting gap structures in both CsV_3Sb_5 and KV_3Sb_5 can be appropriately described by a two-gap s -wave model, consistent with nodeless superconductivity in CsV_3Sb_5 revealed through magnetic penetration depth measurements¹⁸.

Temperature evolution of the differential conductance $G(V)$ curves for SPCS on CsV_3Sb_5 is shown in Fig. 3(a). With increasing temperature, the double peaks gradually shift towards the center, merging into a single zero-bias peak that disappears as temperature approaches T_c . To extract the temperature dependence of the superconducting gaps Δ_1 and Δ_2 , we fit the $G(V)$ curves to the two-gap s -wave BTK model with ω constrained to its value at 0.3 K ($\omega = 0.674$), shown as solid lines in Fig. 3(a). While the two-gap model is clearly

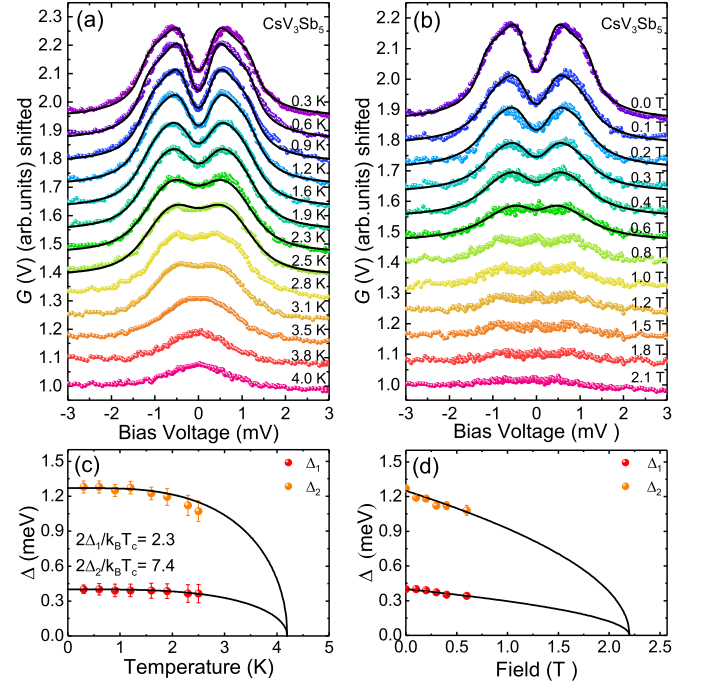


FIG. 3: Normalized differential conductance curves for CsV_3Sb_5 from SPCS, as a function of (a) temperature and (b) magnetic field. The solid lines are fits to the two-gap s -wave BTK model. The extracted superconducting gaps Δ_1 and Δ_2 are shown as a function of (c) temperature with $H = 0$ T and (d) magnetic field with $T = 0.3$ K. The solid lines are based on the BCS theory, with T_c and H_{c2} estimated from the zero-bias conductance.

better than the single-gap model in describing $G(V)$ curves at low temperatures (Fig. 2), for $T \gtrsim 2.5$ K both models can reasonably capture the data. In such a situation, although a two-gap behavior is expected to persist, it is no longer possible to reliably and independently determine Δ_1 and Δ_2 . The extracted values of Δ_1 and Δ_2 from fits in Fig. 3(a) are shown in Fig. 3(c), and the solid black lines are the expected behavior from BCS theory, with $T_c = 4.2$ K inferred from the zero-bias conductance in Fig. 1(a). The superconducting gaps at zero temperature are found to be $\Delta_1 = 0.4$ meV and $\Delta_2 = 1.27$ meV, yielding $2\Delta_1/k_B T_c = 2.3$ and $2\Delta_2/k_B T_c = 7.4$. The larger gap clearly exceeds $2\Delta/k_B T_c = 3.52$ in the weak-coupling limit, while the smaller gap is well below it. Such a behavior is characteristic of two-gap superconductors such as MgB_2 ³⁴, and corroborates the notion that superconductivity in CsV_3Sb_5 is multi-gap in nature.

The magnetic field dependence of $G(V)$ for SPCS on CsV_3Sb_5 at 0.3 K is shown in Fig. 3(b), with field along the c -axis. These data are analyzed using the two-gap BTK model, with results shown in Fig. 3(d). For $H > 0.6$ T, it is no longer possible to independently extract both gaps. The obtained field evolution of the two gaps Δ_1 and Δ_2 reasonably follow $\Delta = \Delta(0)(1 - H/H_{c2})^{1/2}$ (solid black lines), expected for type-II superconductors in the vortex state³⁵. The upper critical field H_{c2} is

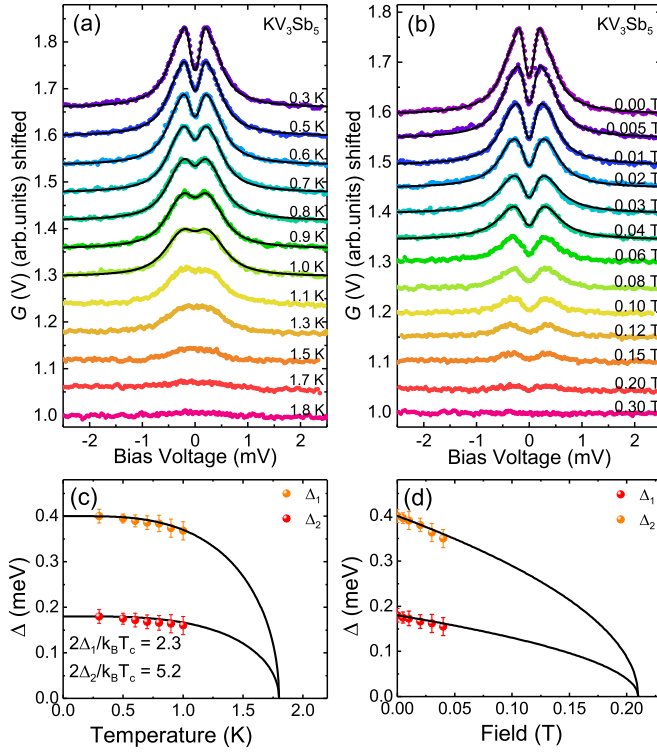


FIG. 4: Normalized differential conductance curves for KV_3Sb_5 from SPCS, as a function of (a) temperature and (b) magnetic field. The solid lines are fits to the two-gap s -wave BTK model. The extracted superconducting gaps Δ_1 and Δ_2 are shown as a function of (c) temperature with $H = 0$ T and (d) magnetic field with $T = 0.3$ K. The solid lines are based on the BCS theory, with T_c and H_{c2} estimated from the zero-bias conductance.

estimated to be ≈ 2.2 T from the field-dependence of the zero-bias conductance [Fig. 1(c)].

Similar SPCS measurements were carried out for KV_3Sb_5 , with results shown in Fig. 4. The differential conductance curves at different temperatures show that they flatten above ≈ 1.8 K [Fig. 4(a)], significantly above $T_c = 1.0$ K from specific heat. For KV_3Sb_5 , the values of Δ_1 and Δ_2 can be reliably extracted for $T \leq 1.0$ K ($H = 0$ T) and $H \leq 0.04$ T ($T = 0.3$ K), with extracted values shown in Figs. 4(c) and (d), respectively. The temperature and field evolution of the two gaps are consistent with expectations of the BCS theory, with $T_c = 1.8$ K and $H_{c2} = 0.21$ T determined from the zero-bias conductance [Figs. 1(b) and (d)]. From the extracted gap values, we find $2\Delta_1/k_B T_c = 2.3$ and $2\Delta_2/k_B T_c = 5.2$, similar to CsV_3Sb_5 .

C. Differential conductance curves from MPCS

In order to have a comparative study of how strain affects the superconducting state of AV_3Sb_5 , we applied MPCS to study both CsV_3Sb_5 and KV_3Sb_5 , with results shown in Fig. 5 for CsV_3Sb_5 and Fig. 6 for KV_3Sb_5 . In the case of CsV_3Sb_3 , we find the measured differential

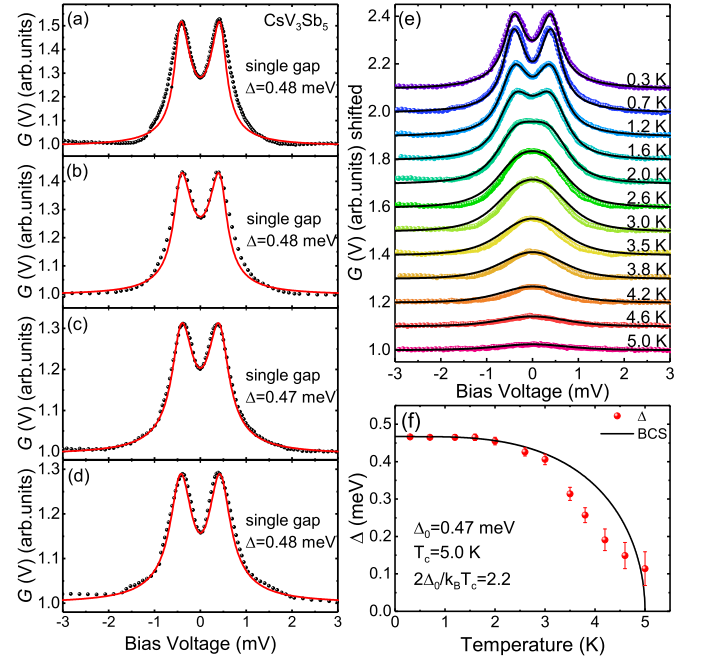


FIG. 5: (a)-(d) Representative MPCS differential conductance curves for CsV_3Sb_5 at $T = 0.3$ K. The red solid line are fits to a single-gap s -wave BTK model. (e) Temperature evolution of the MPCS differential conductance curves for CsV_3Sb_5 , fit to a single-gap s -wave BTK model (black solid lines). (f) Temperature dependence of the extracted superconducting gap Δ from (e), the black line is the expected behavior of the BCS theory, with $\Delta_0 = 0.47$ meV and $T_c = 5.0$ K ($2\Delta_0/k_B T_c = 2.2$).

conductance curves can be reasonably fit by a single-gap s -wave model [Figs. 6(a)-(d)], with $\Delta \approx 0.47$ meV. However, from the zero-bias conductance [Fig. 1(a)] and temperature-dependent conductance curves [Fig. 5(e)], we find $T_c \approx 5.0$ K, which leads to $2\Delta/k_B T_c \approx 2.2$. This value is significantly smaller than the BCS weak-coupling limit of 3.52, but is similar to $2\Delta_1/k_B T_c \approx 2.3$ from SPCS measurements on CsV_3Sb_5 . This implies the presence of a larger gap in MPCS measurements, which is undetected due to a diminishing spectral weight. By analyzing the differential conductance curves with the single-gap s -wave model, we find the temperature dependence of Δ clearly deviates from BCS theory [Fig. 5(f)], characteristic of the smaller gap in some two-gap superconductors^{36,37}.

Similar behaviors are found for MPCS on KV_3Sb_5 , as shown in Fig. 6. The differential conductance curves are also reasonably accounted for using a single-gap s -wave model, with $\Delta \approx 0.34$ meV [Figs. 6(a)-(d)]. Combined with $T_c \approx 3.1$ K from Figs. 1(b) and 6(e), we obtain $2\Delta/k_B T_c \approx 2.5$, also significantly smaller than 3.52, and clear deviations of Δ from the BCS theory is also observed in its temperature evolution. Our MPCS measurements suggest that CsV_3Sb_5 and KV_3Sb_5 are similar, and both exhibit multi-gap superconductivity, although the larger gap is undetected likely due to a diminished spectral weight.

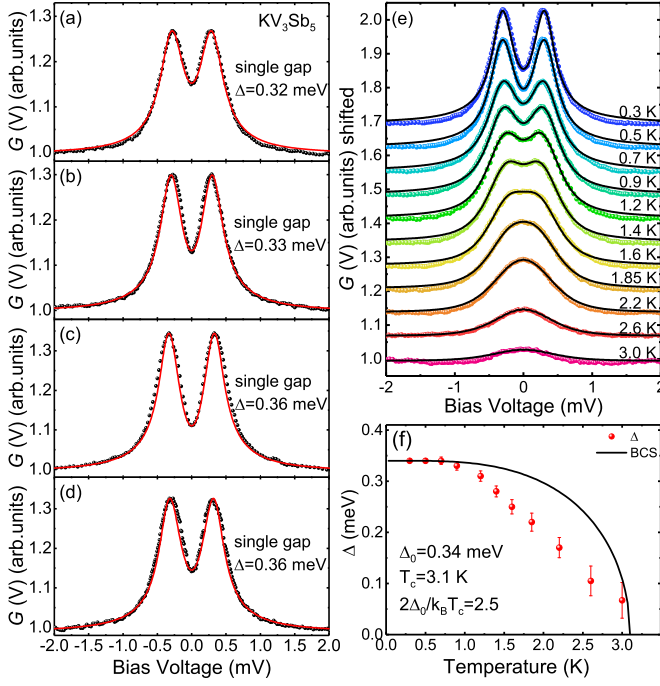


FIG. 6: (a)-(d) Representative MPCS differential conductance curves for KV_3Sb_5 at $T = 0.3$ K. The solid red lines are fits to a single-gap s -wave BTK model. (e) Temperature evolution of the MPCS differential conductance curves for KV_3Sb_5 , fit to a single-gap s -wave BTK model (black solid lines). (f) Temperature dependence of the extracted superconducting gap Δ from (e), the black line is the expected behavior of the BCS theory, with $\Delta_0 = 0.34$ meV and $T_c = 3.1$ K ($2\Delta_0/k_B T_c = 2.5$).

IV. DISCUSSION AND CONCLUSION

All differential conductance curves in Figs. 2-6 from SPCS and MPCS can be consistently described by a two-gap s -wave model, although extracting the values of the two gaps may be hindered by the diminishing spectral weight of the larger gap in MPCS measurements. Our results therefore favor nodeless multi-gap superconductivity in the AV_3Sb_5 series, and suggest that the structure of the superconducting order parameter remains robust when T_c becomes strongly enhanced. This is consistent with the observation of an exponential temperature dependence of the magnetic penetration depth¹⁸, a Hebel-Slichter coherence peak from nuclear magnetic resonance¹⁹, and sensitivity of the superconducting state to magnetic impurities from scanning tunneling microscopy measurements²⁰. However, it should be noted that a robust nodal superconducting state has been suggested by thermal conductivity measurements¹⁷, and supported by certain theoretical considerations²¹.

In point-contact spectroscopy measurements on layered materials, perfectly two-dimensional Fermi sheets do not contribute to the differential conductance for point-contact in the c -axis direction. As a Fermi surface becomes progressively more corrugated

along the c -axis direction, its spectral weight in the differential conductance increases in tandem. Therefore, the differing spectral weight of the large and small superconducting gaps between SPCS and MPCS measurements may correspond to varying degrees of out-of-plane dispersion in the normal state electronic structures. In this scenario, the small spectral weight of the larger gap in MPCS measurements suggests that the larger strain in MPCS measurements leads to the corresponding band becoming more two-dimensional compared to SPCS measurements, and points to a nontrivial effect of strain on the normal state electronic structure of AV_3Sb_5 .

For SPCS measurements, local stress or strain may arise during curing of the silver paste or upon cooling due to differential thermal contraction between the sample and the silver paste. As these effects are usually weak, they can be ignored in most SPCS measurements. However, given the tendency of AV_3Sb_5 crystals to exfoliate, lateral stress could be limited to a few layers near the surface, which can induce a sizable strain even if the stress is small. Such sizable strains coupled with the sensitivity to pressure (and thus strain)^{17,26-30}, likely accounts for the enhanced superconductivity observed in CsV_3Sb_5 and KV_3Sb_5 from our SPCS measurements. In addition, as AV_3Sb_5 are good metals with a large density of states at the Fermi level, charge doping through the silver paste should play a minor role in enhancing superconductivity. In contrast, both strain effects and charge doping may be operative in the dramatic enhancement of T_c seen in $MoTe_2$ from SPCS measurements³⁸, as $MoTe_2$ is a semi-metal with superconductivity sensitive to pressure³⁹.

Compared to SPCS, a more significant strain is typically applied by the sharp tip in MPCS measurements, consistent with the more significant increase in T_c . It should be noted that whereas strain is dominantly in the ab -plane for SPCS, it is mostly along the c -axis for MPCS. The observation of enhanced T_c in both approaches then indicates superconductivity in AV_3Sb_5 is sensitive to strain in more than one symmetry channel, and motivates further studies on the evolution of superconductivity in AV_3Sb_5 under uniaxial strain. In addition, since the c -axis collapses more readily under hydrostatic pressure²⁹, the large susceptibility of the crystal structure to c -axis stress may also contribute to the stronger effect of mechanical point-contact on superconductivity. A dramatic increase in T_c was also reported in $FeSe$ through MPCS measurements⁴⁰, which is also a highly two-dimensional material with superconductivity that becomes enhanced under hydrostatic pressure^{41,42}. Taking the results on AV_3Sb_5 , $MoTe_2$ and $FeSe$ together, it appears that layered materials with superconductivity that becomes enhanced under hydrostatic pressure are susceptible to strain effects in point-contact spectroscopy measurements.

Compared to hydrostatic pressure, strain is much

easier to realize and manipulate in devices, giving it a unique advantage in practical applications. Our results demonstrate that local strain from point-contacts are sufficient to dramatically tune the superconducting properties of AV_3Sb_5 , and suggests that such strain-sensitive superconductivity may be useful in device engineering, for example, in realizing superconductor-metal heterostructures. Furthermore, strain may be utilized in the manipulation of possible Majorana zero modes in these materials²³.

In conclusion, we performed SPCS and MPCS measurements on CsV_3Sb_5 and KV_3Sb_5 , and observed enhanced superconductivity in all cases. This enhancement likely originates from local strain induced by the point-contacts, since similar enhancements are absent in scanning tunneling microscopy measurements. While the superconducting gap structure is better described by a two-gap *s*-wave model for SPCS results (as in MgB_2), a single-gap BTK model can reasonably capture the MPCS results, pointing to a nontrivial evolution of the normal state electronic structure upon

strain-tuning. Our findings highlight the sensitivity of superconductivity to strain in the kagome metals AV_3Sb_5 , which may be useful in the device-engineering of these materials.

We are grateful for valuable discussions with C. Cao and Y. Liu. The work at Zhejiang University was supported by the National Key R&D Program of China (No. 2017YFA0303100, No. 2016YFA0300202), the Key R&D Program of Zhejiang Province, China (2021C01002), the National Natural Science Foundation of China (No. 11674279, No. 11974306 and No. 12034017), and the Fundamental Research Funds for the Central Universities of China. X.L. would like to acknowledge support from the Zhejiang Provincial Natural Science Foundation of China (LR18A04001). S.D.W. and B.R.O. gratefully acknowledge support via the UC Santa Barbara NSF Quantum Foundry funded via the Q-AMASE-i program under award DMR-1906325. B.R.O. also acknowledges support from the California NanoSystems Institute through the Elings fellowship program.

-
- * These authors have contributed equally to this work.
† Corresponding author: yusong_phys@zju.edu.cn
‡ Corresponding author: xinluphy@zju.edu.cn
- ¹ L. Ye, M. Kang, J. Liu, F. von Cube, C. R. Wicker, T. Suzuki, C. Jozwiak, A. Bostwick, E. Rotenberg, D. C. Bell, et al., *Nature* **555**, 638 (2018), URL <https://doi.org/10.1038/nature25987>.
 - ² E. Liu, Y. Sun, N. Kumar, L. Muechler, A. Sun, L. Jiao, S.-Y. Yang, D. Liu, A. Liang, Q. Xu, et al., *Nature Physics* **14**, 1125 (2018), URL <https://doi.org/10.1038/s41567-018-0234-5>.
 - ³ M. Kang, L. Ye, S. Fang, J.-S. You, A. Levitan, M. Han, J. I. Facio, C. Jozwiak, A. Bostwick, E. Rotenberg, et al., *Nature Materials* **19**, 163 (2019), URL <https://doi.org/10.1038/s41563-019-0531-0>.
 - ⁴ J.-X. Yin, W. Ma, T. A. Cochran, X. Xu, S. S. Zhang, H.-J. Tien, N. Shumiya, G. Cheng, K. Jiang, B. Lian, et al., *Nature* **583**, 533 (2020), URL <https://doi.org/10.1038/s41586-020-2482-7>.
 - ⁵ W.-S. Wang, Z.-Z. Li, Y.-Y. Xiang, and Q.-H. Wang, *Phys. Rev. B* **87**, 115135 (2013), URL <https://link.aps.org/doi/10.1103/PhysRevB.87.115135>.
 - ⁶ S. V. Isakov, S. Wessel, R. G. Melko, K. Sengupta, and Y. B. Kim, *Phys. Rev. Lett.* **97**, 147202 (2006), URL <https://link.aps.org/doi/10.1103/PhysRevLett.97.147202>.
 - ⁷ H.-M. Guo and M. Franz, *Phys. Rev. B* **80**, 113102 (2009), URL <https://link.aps.org/doi/10.1103/PhysRevB.80.113102>.
 - ⁸ M. L. Kiesel, C. Platt, and R. Thomale, *Phys. Rev. Lett.* **110**, 126405 (2013), URL <https://link.aps.org/doi/10.1103/PhysRevLett.110.126405>.
 - ⁹ J. Wen, A. Rüegg, C.-C. J. Wang, and G. A. Fiete, *Phys. Rev. B* **82**, 075125 (2010), URL <https://link.aps.org/doi/10.1103/PhysRevB.82.075125>.
 - ¹⁰ T. Park, M. Ye, and L. Balents, arXiv:2104.08425 (2021), URL <https://arxiv.org/abs/2104.08425v2>.
 - ¹¹ B. R. Ortiz, L. C. Gomes, J. R. Morey, M. Winiarski, M. Bordelon, J. S. Mangum, I. W. H. Oswald, J. A. Rodriguez-Rivera, J. R. Neilson, S. D. Wilson, et al., *Phys. Rev. Materials* **3**, 094407 (2019), URL <https://link.aps.org/doi/10.1103/PhysRevMaterials.3.094407>.
 - ¹² B. R. Ortiz, S. M. L. Teicher, Y. Hu, J. L. Zuo, P. M. Sarte, E. C. Schueller, A. M. M. Abeykoon, M. J. Krogstad, S. Rosenkranz, R. Osborn, et al., *Phys. Rev. Lett.* **125**, 247002 (2020), URL <https://link.aps.org/doi/10.1103/PhysRevLett.125.247002>.
 - ¹³ B. R. Ortiz, P. M. Sarte, E. M. Kenney, M. J. Graf, S. M. L. Teicher, R. Seshadri, and S. D. Wilson, *Phys. Rev. Materials* **5**, 034801 (2021), URL <https://link.aps.org/doi/10.1103/PhysRevMaterials.5.034801>.
 - ¹⁴ Q. Yin, Z. Tu, C. Gong, Y. Fu, S. Yan, and H. Lei, *Chinese Physics Letters* **38**, 037403 (2021), URL <https://doi.org/10.1088/0256-307x/38/3/037403>.
 - ¹⁵ Y.-X. Jiang, J.-X. Yin, M. M. Denner, N. Shumiya, B. R. Ortiz, G. Xu, Z. Guguchia, J. He, M. S. Hossain, X. Liu, et al., *Nature Materials* (2021), URL <https://doi.org/10.1038/s41563-021-01034-y>.
 - ¹⁶ X. Feng, K. Jiang, Z. Wang, and J. Hu, *Science Bulletin* p. in press (2021), ISSN 2095-9273, URL <http://dx.doi.org/10.1016/j.scib.2021.04.043>.
 - ¹⁷ C. C. Zhao, L. S. Wang, W. Xia, Q. W. Yin, J. M. Ni, Y. Y. Huang, C. P. Tu, Z. C. Tao, Z. J. Tu, C. S. Gong, et al., arXiv:2102.08356 (2021), URL <https://arxiv.org/abs/2102.08356>.
 - ¹⁸ W. Duan, Z. Nie, S. Luo, F. Yu, B. R. Ortiz, L. Yin, H. Su, F. Du, A. Wang, Y. Chen, et al., arXiv:2103.11796 (2021), URL <https://arxiv.org/abs/2103.11796v1>.
 - ¹⁹ C. Mu, Q. Yin, Z. Tu, C. Gong, H. Lei, Z. Li, and J. Luo, arXiv:2104.06698 (2021), URL <https://arxiv.org/abs/2104.06698v1>.
 - ²⁰ H.-S. Xu, Y.-J. Yan, R. Yin, W. Xia, S. Fang, Z. Chen, Y. Li, W. Yang, Y. Guo, and D.-L. Feng, arXiv:2104.08810 (2021), URL <https://arxiv.org/abs/2104.08810v1>.
 - ²¹ X. Wu, T. Schwemmer, T. Müller, A. Consiglio,

- G. Sangiovanni, D. D. Sante, Y. Iqbal, W. Hanke, A. P. Schnyder, M. M. Denner, et al., arXiv:2104.05671 (2021), URL <https://arxiv.org/abs/2104.05671v1>.
- ²² Y. Wang, S. Yang, P. K. Sivakumar, B. R. Ortiz, S. M. L. Teicher, H. Wu, A. K. Srivastava, C. Garg, D. Liu, S. S. P. Parkin, et al., arXiv:2012.05898 (2020), URL <https://arxiv.org/abs/2012.05898v2>.
- ²³ Z. Liang, X. Hou, W. Ma, F. Zhang, P. Wu, Z. Zhang, F. Yu, J. J. Ying, K. Jiang, L. Shan, et al., arXiv:2103.04760 (2021), URL <https://arxiv.org/abs/2103.04760v3>.
- ²⁴ S. D. Sarma, M. Freedman, and C. Nayak, npj Quantum Information **1**, 15001 (2015), URL <https://doi.org/10.1038/npjqi.2015.1>.
- ²⁵ M. Sato and Y. Ando, Reports on Progress in Physics **80**, 076501 (2017), URL <https://doi.org/10.1088/1361-6633/aa6ac7>.
- ²⁶ K. Y. Chen, N. N. Wang, Q. W. Yin, Y. H. Gu, K. Jiang, Z. J. Tu, C. S. Gong, Y. Uwatoko, J. P. Sun, H. C. Lei, et al., Phys. Rev. Lett. **126**, 247001 (2021), URL <https://link.aps.org/doi/10.1103/PhysRevLett.126.247001>.
- ²⁷ F. Du, S. Luo, B. R. Ortiz, Y. Chen, W. Duan, D. Zhang, X. Lu, S. D. Wilson, Y. Song, and H. Yuan, Phys. Rev. B **103**, L220504 (2021), URL <https://link.aps.org/doi/10.1103/PhysRevB.103.L220504>.
- ²⁸ F. Yu, D. Ma, W. Zhuo, S. Liu, X. Wen, B. Lei, J. Ying, and X. Chen, Nature Communications **12**, 3645 (2021), URL <https://doi.org/10.1038/s41467-021-23928-w>.
- ²⁹ Z. Zhang, Z. Chen, Y. Zhou, Y. Yuan, S. Wang, J. Wang, H. Yang, C. An, L. Zhang, X. Zhu, et al., Phys. Rev. B **103**, 224513 (2021), URL <https://link.aps.org/doi/10.1103/PhysRevB.103.224513>.
- ³⁰ C. C. Zhu, X. F. Yang, W. Xia, Q. W. Yin, L. S. Wang, C. C. Zhao, D. Z. Dai, C. P. Tu, B. Q. Song, Z. C. Tao, et al., arXiv:2104.14487 (2021), URL <https://arxiv.org/abs/2104.14487v1>.
- ³¹ H. Chen, H. Yang, B. Hu, Z. Zhao, J. Yuan, Y. Xing, G. Qian, Z. Huang, G. Li, Y. Ye, et al., arXiv:2103.09188 (2021), URL <https://arxiv.org/abs/2103.09188v1>.
- ³² S. Ni, S. Ma, Y. Zhang, J. Yuan, H. Yang, Z. Lu, N. Wang, J. Sun, Z. Zhao, D. Li, et al., Chinese Physics Letters **38**, 057403 (2021), URL <https://doi.org/10.1088/0256-307x/38/5/057403>.
- ³³ G. Sheet, S. Mukhopadhyay, and P. Raychaudhuri, Phys. Rev. B **69**, 134507 (2004), URL <https://link.aps.org/doi/10.1103/PhysRevB.69.134507>.
- ³⁴ A. Brinkman, A. A. Golubov, H. Rogalla, O. V. Dolgov, J. Kortus, Y. Kong, O. Jepsen, and O. K. Andersen, Phys. Rev. B **65**, 180517 (2002), URL <https://link.aps.org/doi/10.1103/PhysRevB.65.180517>.
- ³⁵ E. Brandt, physica status solidi (b) **77**, 105 (1976), URL <https://doi.org/10.1002/pssb.2220770109>.
- ³⁶ P. Szabó, P. Samuely, J. Kačmarčík, T. Klein, J. Marcus, D. Fruchart, S. Miraglia, C. Marcenat, and A. G. M. Jansen, Phys. Rev. Lett. **87**, 137005 (2001), URL <https://link.aps.org/doi/10.1103/PhysRevLett.87.137005>.
- ³⁷ R. S. Gonnelli, D. Daghero, G. A. Ummarino, V. A. Stepanov, J. Jun, S. M. Kazakov, and J. Karpinski, Phys. Rev. Lett. **89**, 247004 (2002), URL <https://link.aps.org/doi/10.1103/PhysRevLett.89.247004>.
- ³⁸ Y. Naidyuk, O. Kvitnitskaya, D. Bashlakov, S. Aswartham, I. Morozov, I. Chernyavskii, G. Fuchs, S.-L. Drechsler, R. Hühne, and K. Nielsch, 2D Materials **5**, 045014 (2018), URL <https://doi.org/10.1088/2053-1583/aad3e2>.
- ³⁹ Y. Qi, P. G. Naumov, M. N. Ali, C. R. Rajamathi, W. Schnelle, O. Barkalov, M. Hanfland, S.-C. Wu, C. Shekhar, Y. Sun, et al., Nature Communications **7**, 11038 (2016), URL <https://doi.org/10.1038/ncomms11038>.
- ⁴⁰ Y. G. Naidyuk, G. Fuchs, D. A. Chareev, and A. N. Vasiliev, Phys. Rev. B **93**, 144515 (2016), URL <https://link.aps.org/doi/10.1103/PhysRevB.93.144515>.
- ⁴¹ S. Medvedev, T. M. McQueen, I. A. Troyan, T. Palasyuk, M. I. Erements, R. J. Cava, S. Naghavi, F. Casper, V. Ksenofontov, G. Wortmann, et al., Nature Materials **8**, 630 (2009), URL <https://doi.org/10.1038/nmat2491>.
- ⁴² S. Margadonna, Y. Takabayashi, Y. Ohishi, Y. Mizuguchi, Y. Takano, T. Kagayama, T. Nakagawa, M. Takata, and K. Prassides, Phys. Rev. B **80**, 064506 (2009), URL <https://link.aps.org/doi/10.1103/PhysRevB.80.064506>.